



## B-KUL-H04X3A: Control Theory

**Team 47:**

Lefebure Tiebert (r0887630)  
Campaert Lukas (r0885501)

# Assignment 2: Velocity control of the cart

**Professor:**

Prof. Dr. Ir. Jan Swevers

Academic Year 2025-2026

## ***Declaration of Originality***

We hereby declare that this submitted draft is entirely our own, subject to feedback and support given us by the didactic team, and subject to lawful cooperation which was agreed with the same didactic team. Regarding this draft, we also declare that:

1. Note has been taken of the text on academic integrity <https://eng.kuleuven.be/studeren/mastoproef-en-papers/documenten/20161221-academische-integriteit-okt2016.pdf>.
2. No plagiarism has been committed as described on <https://eng.kuleuven.be/studeren/mastoproef-en-papers/plagiaat#Definitie: Wat is plagiaat?>.
3. All experiments, tests, measurements, . . . , have been performed as described in this draft, and no data or measurement results have been manipulated.
4. All sources employed in this draft – including internet sources – have been correctly referenced.

# 1 Velocity controller design using the frequency response method

## 1.1 Controller type choice (1a)

To achieve zero steady-state error on a constant velocity reference, which requires a closed-loop system with type 1 behaviour, the controller must provide infinite DC gain. The identified DC-motor dynamics contain no inherent integrator, meaning proportional (P), proportional-derivative (PD), or lead-type controllers would leave a nonzero steady-state error.

Desired closed-loop properties include: zero steady-state error on a constant velocity reference, adequate robustness (sufficient phase margin), sufficient closed-loop bandwidth  $\omega_{BW}$  for accurate velocity tracking, and low sensitivity to external disturbances (e.g. cart on incline, friction).

Possible controller structures:

- P/PD: no integrator (I), meaning a nonzero steady-state error
- lead: increases phase margin  $PM$  but does not provide infinite DC gain
- lag: increases low-frequency gain but insufficient for zero steady-state error
- PI: provides an integrator and a zero for phase correction
- PID: ensures zero steady-state error and can increase phase margin, but the derivative term (D) is sensitive to noise and is therefore avoided in this application

The PI compensator is selected as a suitable controller. The continuous-time transfer function for the PI compensator is [1]:

$$D(s) = \frac{K}{s} \left( s + \frac{1}{T_i} \right), \quad (1)$$

where  $K$  is the proportional gain  $[-]$  and  $T_i$  the integration time  $[s]$ .

The controller increases the system type by 1 and ensures infinite DC gain:

$$\lim_{s \rightarrow 0} D(s) = \infty, \quad (2)$$

which ensures zero steady-state error for step velocity references and offers straightforward tuning in the frequency domain, making it highly suitable for motor velocity control.

## 1.2 Design process and design parameters choices (1b)

The controller parameters are obtained using the frequency-response method, based on the identified motor models from Assignment 1, both for motor A and motor B. The **unfiltered simplified discrete-time models** are:

$$H_A(z) = \frac{0.6309}{z^2 - 0.6819z}, \quad (3)$$

$$H_B(z) = \frac{0.6488}{z^2 - 0.6806z}. \quad (4)$$

Transforming these discrete-time models to continuous-time (with *MATLAB*'s *d2c* command) yields:

$$G_{s,A}(s) = \frac{0.3677s^2 - 147.1s + 1.471e04}{s^2 + 237.1s + 7413}, \quad (5)$$

$$G_{s,B}(s) = \frac{0.3763s^2 - 150.5s + 1.505e04}{s^2 + 237s + 7408}. \quad (6)$$

**Choice of cross-over frequency  $\omega_c$ :** The cross-over frequency  $\omega_c$  determines the closed-loop bandwidth  $\omega_{BW}$ . The design value must balance: faster response vs. actuator limitations, tracking performance vs. noise sensitivity, and stability margin vs. speed.

A phase margin target of  $55^\circ$  was imposed to ensure robust behaviour. The uncompensated phase of the motor model is evaluated to find the frequency satisfying:

$$\phi_G(\omega_c) = -180^\circ + PM + \phi_{PI}(\omega_c), \quad (7)$$

where  $\phi_G(\omega_c)$  is the phase of the uncompensated open-loop system at the target cross-over frequency  $\omega_c$ ,  $PM$  is the desired phase margin (which is selected to be  $55^\circ$ ), and  $\phi_{PI}(\omega_c)$  is the anticipated phase lag of the PI compensator at  $\omega_c$  (which is selected to be  $15^\circ$ ).

This yields the following requirement:

$$\phi_G(\omega_c) = -180^\circ + 55^\circ + 15^\circ = -110^\circ. \quad (8)$$

Figure 13 (*Appendix A*) shows the Bode diagram of the uncompensated open-loop system  $G_s(s)$ , both for motor A and motor B. The cross-over frequency  $\omega_c$  where the phase of the uncompensated open-loop system equals  $-110^\circ$  (or where the phase equals  $-110 + 360^\circ = 250^\circ$ ) is the same for both motors, and fixed directly by the specification:

$$\boxed{\omega_{c,A} = \omega_{c,B} = 61.7 \text{ rad/s}.} \quad (9)$$

**Integration time  $T_i$ :** The integrator pole must lie well below the cross-over frequency  $\omega_c$  to avoid excessive phase lag. The integration time is selected such that the contribution of the PI compensator to the phase at  $\omega_c$  equals the anticipated one (this being  $\phi_{PI}(\omega_c) = 15^\circ$ ). This design rule is mathematically expressed as:

$$T_i\omega_c = \tan(90^\circ - \phi_{PI}(\omega_c)), \quad (10)$$

using a margin of  $\phi_{PI}(\omega_c) = 15^\circ$ , leading to:

$$\boxed{T_{i,A} = T_{i,B} = 0.0605 \text{ s}.} \quad (11)$$

**Proportional gain  $K$ :** The proportional gain is calculated such that the gain of the compensated system at the target cross-over frequency  $\omega_c$  equals one:

$$|D(j\omega_c)G_s(j\omega_c)| = 1. \quad (12)$$

The continuous-time controller  $D(s)$  (equation 1) is discretized using the Tustin method (with the *c2d* *MATLAB* command), and the proportional gain  $K$  is adjusted iteratively until *MATLAB*'s Bode diagram confirms the desired cross-over frequency  $\omega_c = 61.7 \text{ rad/s}$ .

Figure 14 (*Appendix A*) illustrates the iterative procedure used to determine the proportional gain  $K$  for both motor A and motor B. Figure 14a shows the compensated open-loop system for motor A where the proportional gain  $K_A$  of the PI compensator is set to 1 (we don't include the gain  $K_A$ ). The gain of the compensated open-loop system does not equal 0 dB at the target cross-over frequency. After some iterative tuning of the gain  $K_A$ , Figure 14b is obtained. The gain of the compensated open-loop system equals 0 dB, exactly at  $\omega_c = 61.7 \text{ rad/s}$ . Figures 14c and 14d show the same iterative process, but for motor B. The identified wheel models yield the following proportional gains:

$$\boxed{K_A = 0.8904, \quad K_B = 0.8663.} \quad (13)$$

Using the identified values of  $K$  and  $T_i$ , the resulting PI controllers for motor A and motor B are given by:

$$D_A(s) = \frac{0.8904}{s}(s + \frac{1}{0.0605}), \quad (14)$$

$$D_B(s) = \frac{0.8663}{s}(s + \frac{1}{0.0605}). \quad (15)$$

**Design trade-offs for controller design parameters ( $PM$ ,  $K$ ,  $T_i$ ,  $\omega_c$ ):**

- increasing  $PM$  provides robustness and damping but slows the response
- increasing  $K$  increases bandwidth but reduces phase margin, raising the risk of oscillatory behaviour and actuator saturation
- increasing  $T_i$  reduces phase lag but slows convergence to steady-state (decreased integral speed)
- increasing  $\omega_c$  reduces delay sensitivity but amplifies encoder noise

**Frequency-domain verification:** The Bode plot for the compensated open-loop system  $L(j\omega) = D(j\omega)G(j\omega)$  must show:

- unity gain ( $|L(j\omega)| = 0 \text{ dB}$ ) at the target cross-over frequency  $\omega_c = 61.7 \text{ rad/s}$ ,
- a phase margin ( $PM$ )  $\approx 55^\circ$ .

The Bode plot for the PI controller  $D(j\omega)$  must show:

- zero located at  $\omega_z = \frac{1}{T_i} = 16.5 \text{ rad/s}$ , far below the target cross-over frequency  $\omega_c$  ( $\omega_z \ll \omega_c$ ).

Finally, the Bode plot for the compensated closed-loop system  $H(j\omega) = \frac{L(j\omega)}{1+L(j\omega)}$  must show:

- closed-loop bandwidth  $\omega_{BW} \approx \omega_c$ ,
- resonant peak caused by finite (moderate) phase margin,
- closed-loop gain rolls off beyond control bandwidth.

Figures 1a and 1b show that, both for motor A (left) and motor B (right), the desired phase margin ( $PM$ ) of  $55^\circ$  is approximately obtained, and the gain of  $L(j\omega)$  is almost equal to  $0 \text{ dB}$  at the target cross-over frequency  $\omega_c$ . The gain margin ( $GM$ ) is also indicated on these plots, which is sufficiently large. In the Bode plot, the  $-180^\circ$  phase crossing occurs at a frequency well above the cross-over frequency  $\omega_c$ . At that higher frequency, the open-loop magnitude is well below  $0 \text{ dB}$ , meaning a substantial increase in gain would be required to reach instability.

Figures 1c and 1d show the PI controller indeed has a zero at  $\omega_z$ . The PI zero is identified at the frequency where the phase equals  $-45^\circ$  and the magnitude is  $3 \text{ dB}$  above the high-frequency gain. Both for motor A (left) and motor B (right), the phase at  $\omega_z$  is approximately  $-45^\circ$ , and the magnitude at  $\omega_z$  is approximately  $3 \text{ dB}$  above the high-frequency plateau  $20\log_{10}K \approx -1 \text{ dB}$ .

Figures 1e and 1f show the desired closed-loop characteristics, both for motor A (left) and motor B (right). The resonant peak near the closed-loop bandwidth  $\omega_{BW}$  is clearly visible, and the gain decreases beyond  $\omega_{BW}$ , indicating attenuation of high-frequency signals.

**Time-domain verification:** The step response of the compensated closed-loop system  $H(s)$  must show:

- zero steady-state error on a constant velocity reference,
- acceptable rise time ( $t_r < 0.5 \text{ s}$ ),
- acceptable overshoot ( $M_p < 20\%$ ).

In Figures 2a and 2b, the step response converges to the reference value in steady-state, demonstrating the effectiveness of the integral action in eliminating the steady-state error, both for motor A (left) and motor B (right). The transient behaviour satisfies the design specifications, with rise time  $t_r$  and overshoot  $M_p$  remaining within the desired limits.

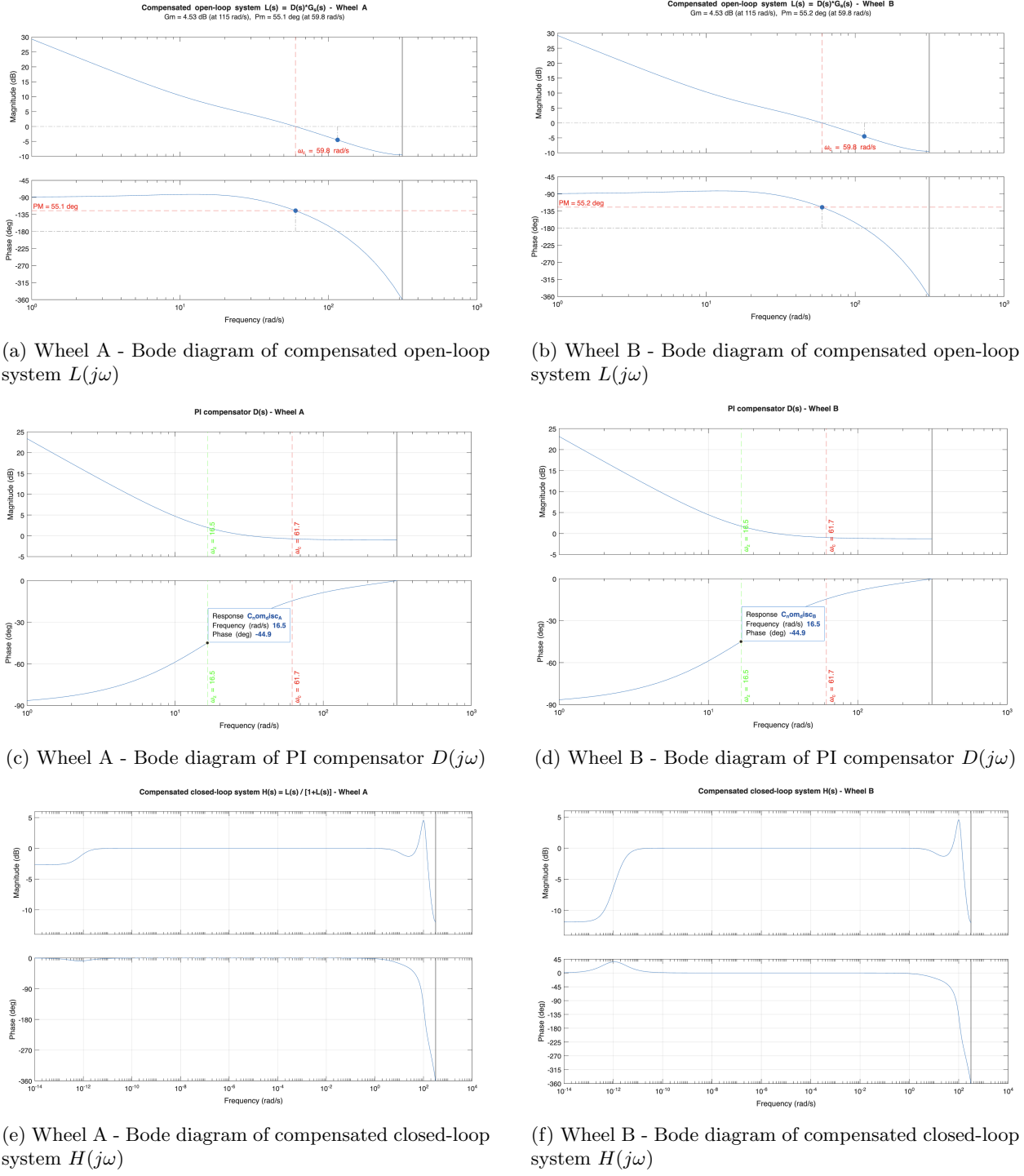


Figure 1: Frequency-domain verification of the designed PI controller for wheel A (left column) and wheel B (right column).

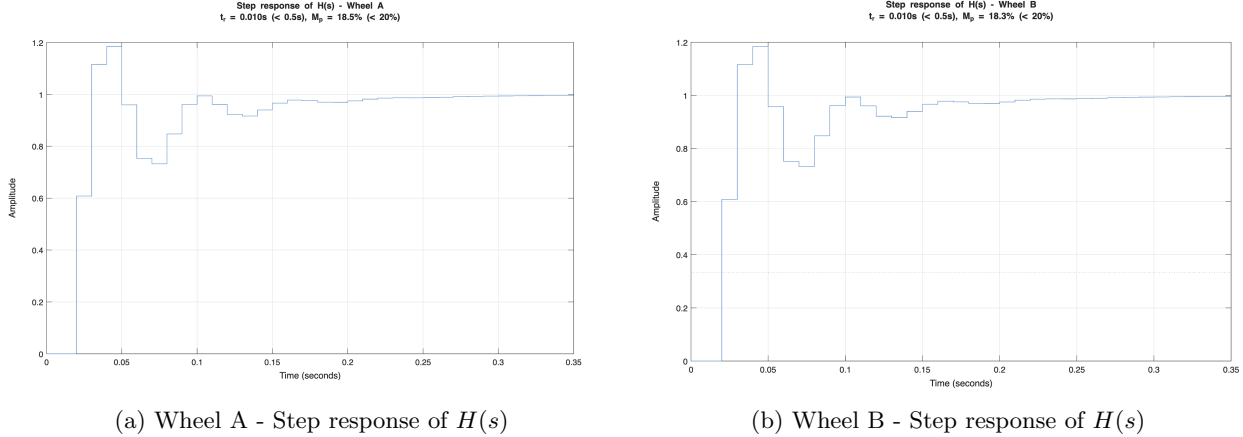


Figure 2: Step response of the compensated closed-loop system  $H(s)$  for wheel A (left) and wheel B (right).

### 1.3 Theoretical and practical closed-loop bandwidth limitations (1c)

**Theoretical limitation:** The closed-loop bandwidth  $\omega_{BW}$  cannot exceed the frequency where the open-loop phase  $\phi_L$  approaches  $-180^\circ$ . Beyond this point, increasing the gain drives the closed-loop system toward instability. For a first-order motor model, this typically limits the cross-over frequency to approximately:

$$\omega_c \approx \frac{1}{\tau}, \quad (16)$$

where  $\tau$  is the motor time constant.

#### Practical limitations:

- sampling frequency (100 Hz): Nyquist limit of 50 Hz ( $= f_s/2$ ) cuts off the maximum achievable bandwidth
- micro-controller delay introduces extra phase lag, reducing stability margins
- voltage saturation (at  $\approx 12$  V) limits the achievable proportional gain
- encoder quantization noise leads to large high-frequency disturbances when the bandwidth is too high
- motor friction and unmodeled nonlinearities reduce agreement with the designed frequency response

These constraints limit the achievable closed-loop bandwidth  $\omega_{BW}$  even if theoretically higher values are possible.

## 2 Experimental validation of the designed controller

### 2.1 Step response validation (2a)

**Experiment:** A constant velocity reference of 10 rad/s is applied to both motors A and B. The measured velocity is compared to the simulated velocity (using the compensated closed-loop model  $H(s)$ ).

**Step response:** Figure 3 shows the closed-loop step response comparison for both motor A (left) and motor B (right). The step reference (dotted line), measured closed-loop response (solid line) and simulated closed-loop response (dashed line) are shown in one plot. The measured and simulated closed-loop responses exhibit similar transient patterns. Initial delays and rise times closely match the model predictions, confirming the validity of the identified motor dynamics. The steady-state velocity converges to the reference value of 10 rad/s, demonstrating correct integral action. Oscillations in the measured signal may be slightly larger than in the simulation due to encoder quantization, unmodeled friction, and voltage saturation clipping. Despite these differences, the measured response remains consistent with expected closed-loop behaviour.

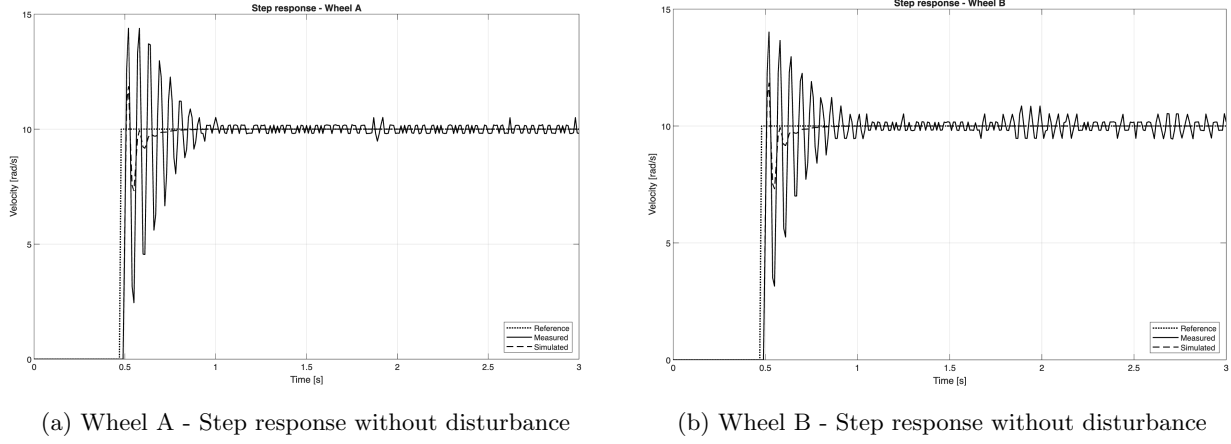


Figure 3: Step response on flat ground for wheel A (left) and wheel B (right): reference (dotted line) vs. measured (solid line) vs. simulated (dashed line).

**Tracking error:** Figure 4 shows the tracking error comparison for both motor A (left) and motor B (right). The measured (solid line) and simulated (dashed line) tracking error of the closed-loop step reference are shown in one plot. The initial tracking error matches the simulated transient and decays to approximately zero, apart from small steady-state fluctuations caused by sensor noise.

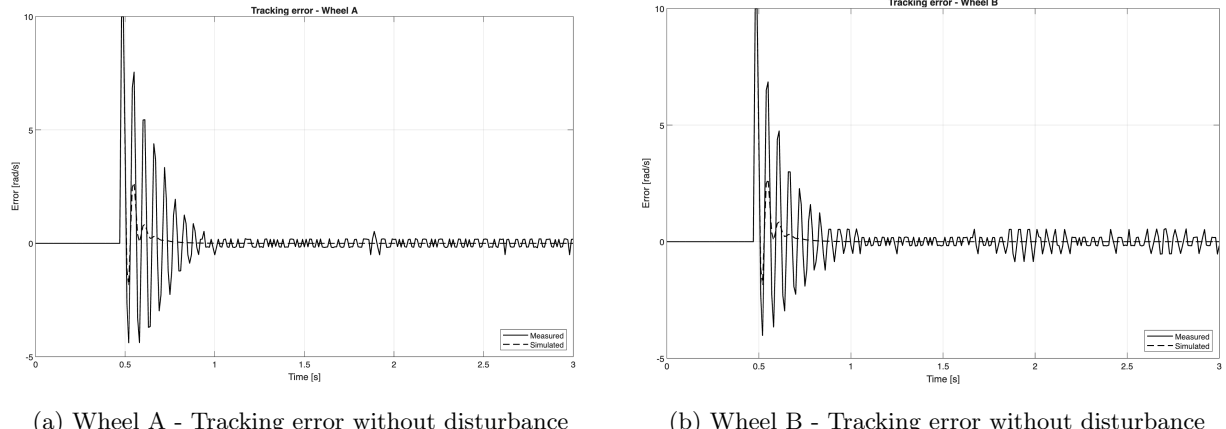


Figure 4: Tracking error on flat ground for wheel A (left) and wheel B (right): measured (solid line) vs. simulated (dashed line).

**Control signal (voltage):** Figure 5 shows the control signal comparison for both motor A (left) and motor B (right). The measured (solid line) and simulated (dashed line) control signal of the closed-loop step reference are shown in one plot. The control voltage initially spikes due to a large tracking error. The measured signal is clipped at roughly 12 V due to hardware limits. This clipping creates a slightly lower first overshoot compared to the simulation. The control signal tracks the evolution of the velocity error as expected.

**Performance characteristics:** Rise time ( $t_r$ ), overshoot ( $M_p$ ) and settling time ( $t_s$ ) align with the design specifications. The measured and simulated responses show closely matching dynamic properties. The rise time  $t_r$  of the measured system is slightly slower than in simulation due to unmodeled friction and voltage saturation, whereas the steady-state value is identical, confirming correct integral action. The overshoot  $M_p$

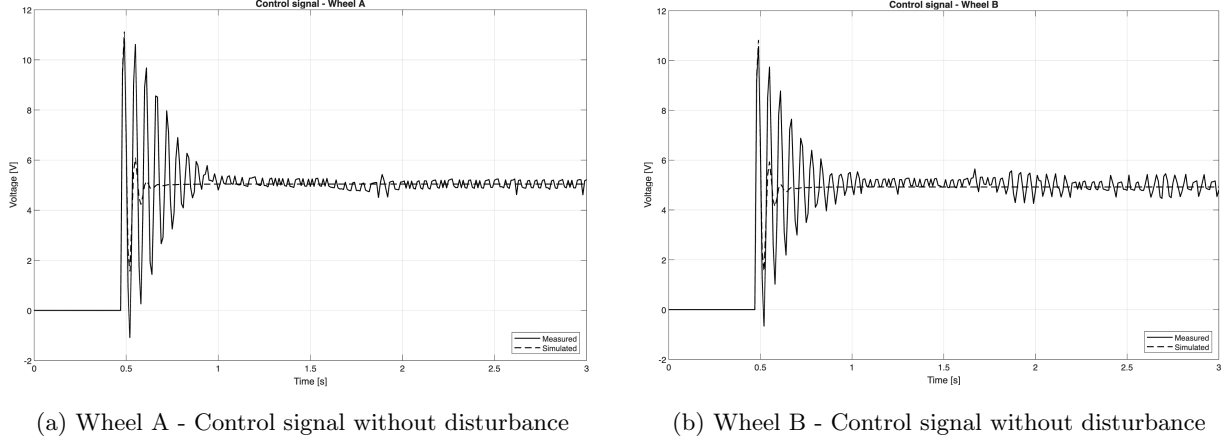


Figure 5: Control voltage on flat ground for wheel A (left) and wheel B (right): measured (solid line) vs. simulated (dashed line). Saturation at  $\approx 12 V$  is visible.

matches well in shape but is marginally larger in the experiment because encoder quantization and actuator limits introduce additional damping and asymmetry. The settling time  $t_s$  remains consistent between measurement and simulation, indicating that the designed phase margin ( $PM = 55^\circ$ ) and bandwidth translate reliably to the real hardware. Overall, the measured performance agrees with the designed characteristics: fast but well-damped convergence, full elimination of steady-state error, and control behaviour that remains within actuator limits.

## 2.2 Steady-state performance under constant force disturbance (2b)

**Experiment:** The cart is placed on an incline so that gravity (constant acceleration  $g = 9.81 \text{ m/s}^2$ ) produces a constant negative torque, opposing the motion, on both wheels. The same velocity setpoint as in Section 2.1 is applied, namely a constant velocity reference of  $10 \text{ rad/s}$ .

**Block diagram:** Figure 6 shows the block diagram of the closed-loop system with the constant force disturbance. The constant force disturbance signal  $f[k]$  enters the loop as an external load torque acting on the motor dynamics  $G[z]$ . The disturbance affects the transient velocity, but the PI controller (the controller dynamics are represented by  $D[z]$ ) gradually compensates through its integral action. The sensor dynamics are represented by  $H[z]$ , and for an ideal sensor,  $H[z] = 1$  (unity feedback).

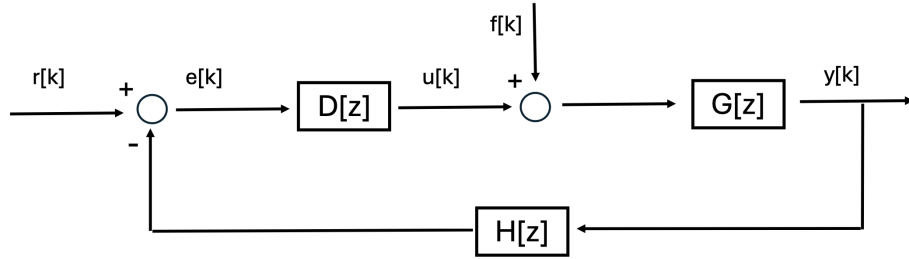
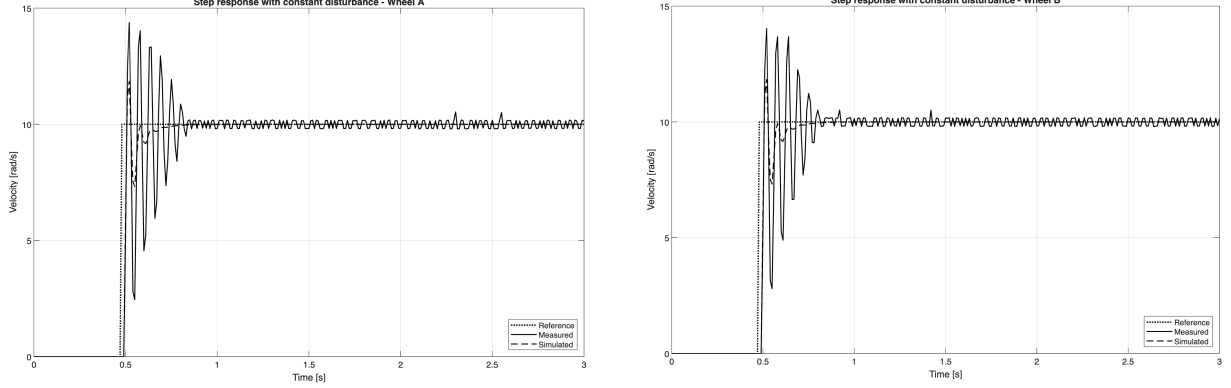


Figure 6: Block diagram of the closed-loop system with the constant force disturbance.

**Step response with constant disturbance:** Figure 7 shows the step response comparison under constant disturbance for both motor A (left) and motor B (right). The step reference (dotted line), measured closed-loop response (solid line) and simulated closed-loop response (dashed line) are shown in one plot. The

measured response shows slightly lower peaks and a slower rise than the nominal case (without disturbance), while the simulated response remains unchanged because it does not include the disturbance. Despite this mismatch in the transient, both measured and simulated curves converge to the same steady-state value due to the integrator, which compensates the constant load.

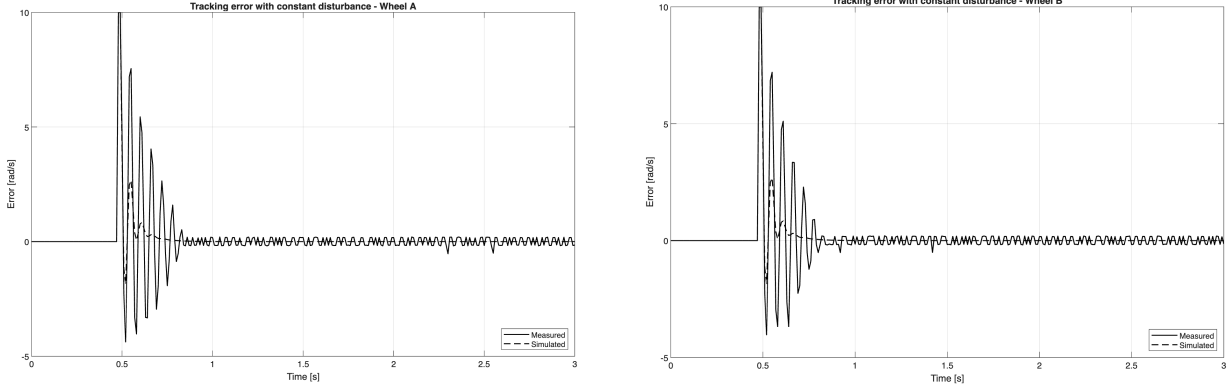


(a) Wheel A - Step response with constant disturbance

(b) Wheel B - Step response with constant disturbance

Figure 7: Step response on the incline for wheel A (left) and wheel B (right): reference (dotted line) vs. measured (solid line) vs. simulated (dashed line).

**Tracking error with constant disturbance:** Figure 8 shows the tracking error comparison with disturbance for both motor A (left) and motor B (right). The measured (solid line) and simulated (dashed line) tracking error of the step reference are shown in one plot. The measured tracking error is larger at the start and decays more smoothly, whereas the simulated error follows the original undisturbed transient. Both measured and simulated tracking error eventually settle close to zero, but only the measured curve reflects the effect of the disturbance.



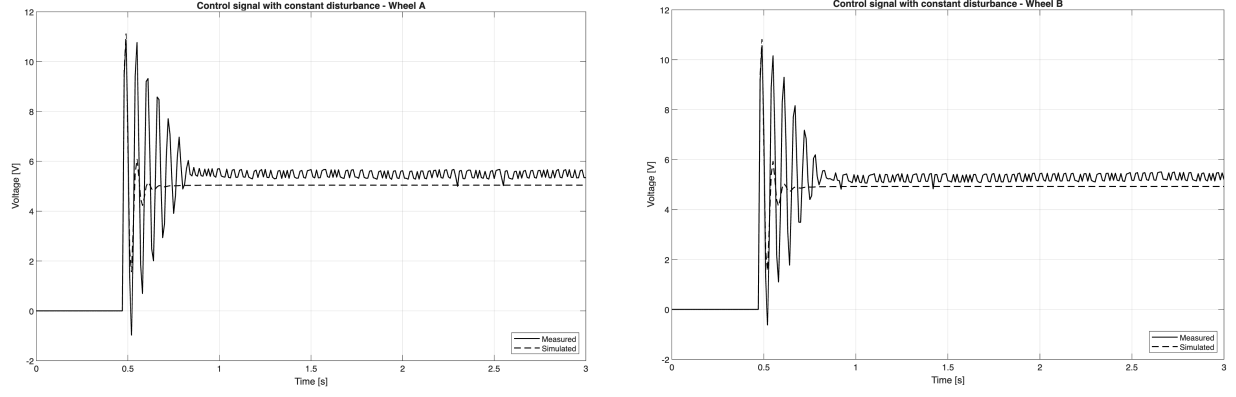
(a) Wheel A - Tracking error with constant disturbance

(b) Wheel B - Tracking error with constant disturbance

Figure 8: Tracking error with constant disturbance for wheel A (left) and wheel B (right): measured (solid line) vs. simulated (dashed line).

**Control signal with constant disturbance:** Figure 9 shows the control signal comparison with disturbance for both motor A (left) and motor B (right). The measured (solid line) and simulated (dashed line) control signal of the step reference are shown in one plot. The measured control signal settles at a visibly higher steady-state value than the simulated one, which remains unchanged without the disturbance term.

The transient shapes remain similar, but only the measured control effort compensates for the additional load.



(a) Wheel A - Control signal with constant disturbance      (b) Wheel B - Control signal with constant disturbance

Figure 9: Control voltage with constant disturbance for wheel A (left) and wheel B (right): measured (solid line) vs. simulated (dashed line).

**Reference tracking despite disturbance:** The controller continues to track the reference in steady-state because the integral action of the PI controller compensates any constant disturbance by increasing the steady-state control effort until the velocity error becomes zero again. Although the transient response is slowed down by the opposing force/torque, the integrator removes the steady-state error for constant disturbances, so the reference is still tracked.

### 2.3 Controller design and validation with cross-over frequency of 0.5 Hz, under constant force disturbance (2c)

**Experiment:** With the redesigned PI controller, the cross-over frequency  $\omega_c$  is reduced to about 0.5 Hz or

$$\boxed{\omega_c^{low-BW} \approx 3.14 \text{ rad/s}}, \quad (17)$$

which lowers the closed-loop bandwidth  $\omega_{BW}$  and yields a more conservative controller. The complete design procedure described in Section 1.2 is repeated for the low-bandwidth controller. Using the identified values of the proportional gain  $K$

$$\boxed{K_A^{low-BW} = 0.4886, \quad K_B^{low-BW} = 0.4771}, \quad (18)$$

and integration time

$$\boxed{T_{i,A}^{low-BW} = T_{i,B}^{low-BW} = 1.1879 \text{ s}}, \quad (19)$$

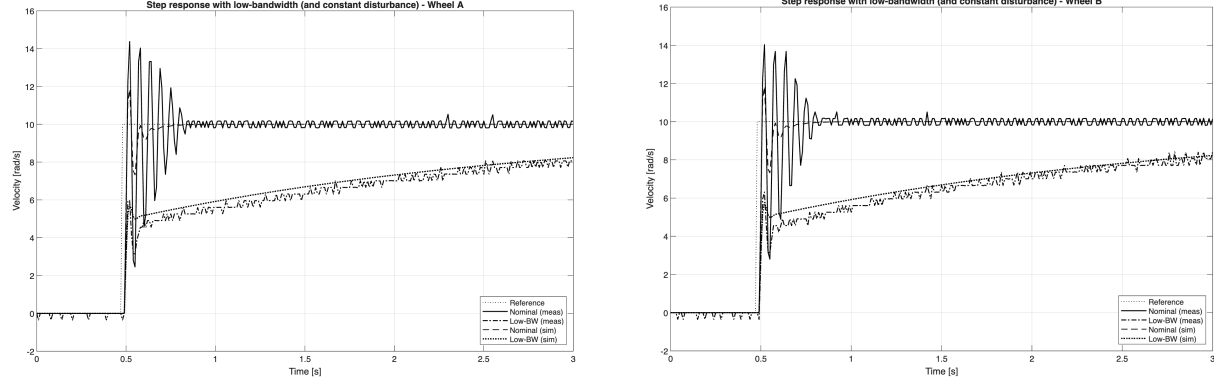
the resulting low-bandwidth PI controllers for motor A and motor B are given by:

$$D_A^{low-BW}(s) = \frac{0.4886}{s} \left( s + \frac{1}{1.1879} \right), \quad (20)$$

$$D_B^{low-BW}(s) = \frac{0.4771}{s} \left( s + \frac{1}{1.1879} \right). \quad (21)$$

The same constant force disturbance (cart on a ramp) is applied and the plots of step response, tracking error and control signal now contain both controllers (nominal controller from Section 2.2 and low-bandwidth controller from Section 2.3). Again, the same velocity setpoint (a constant velocity reference of 10 rad/s) is applied.

**Step response with low-bandwidth (and constant disturbance):** Figure 10 shows the closed-loop step response comparison for both motor A (left) and motor B (right). The step reference (thin dotted line), measured closed-loop response and simulated closed-loop response are shown in one plot, both for the nominal and low-bandwidth case. The measured response with the low-bandwidth controller rises visibly slower and shows almost no overshoot, whereas the nominal controller from Section 2.2 reacts faster and exhibits more pronounced transient peaks. The simulated curves follow the same trend for each controller, but differences between measured and simulated responses remain slightly larger for the nominal case because it is more sensitive to model errors and disturbance effects.



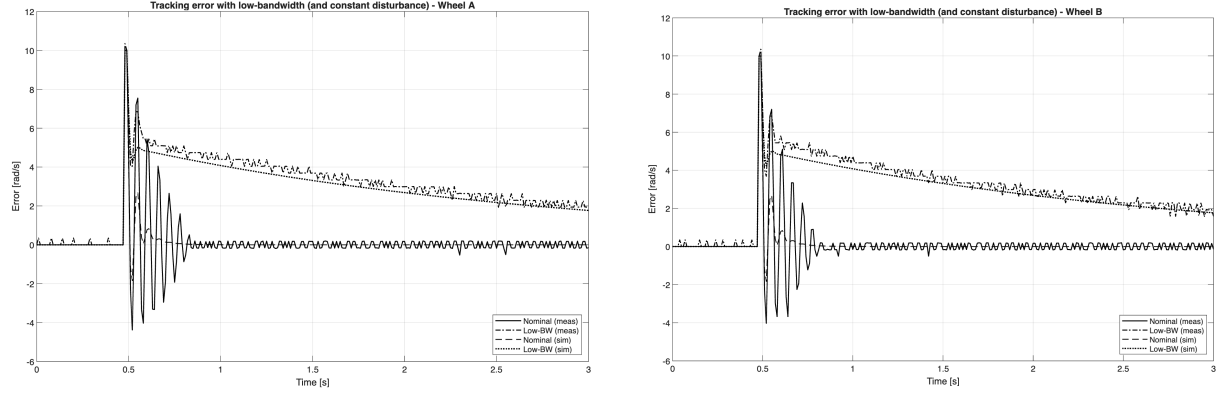
(a) Wheel A - Step response with low-bandwidth (and constant disturbance) (b) Wheel B - Step response with low-bandwidth (and constant disturbance)

Figure 10: Step response comparison for wheel A (left) and wheel B (right): nominal controller vs. low-bandwidth controller, both under constant force disturbance.

**Tracking error with low-bandwidth (and constant disturbance):** Figure 11 shows the tracking error comparison for both motor A (left) and motor B (right). The measured and simulated tracking error of the step reference are shown in one plot, both for the nominal and low-bandwidth case. For the low-bandwidth controller the tracking error decreases more gradually with a smooth, almost aperiodic decay and small oscillations, while the nominal controller produces a quicker error reduction but with larger overshoot and ringing. In both cases the steady-state tracking error remains close to zero, confirming that the integral action compensates the constant disturbance. The low-bandwidth controller, however, needs more time to eliminate the error.

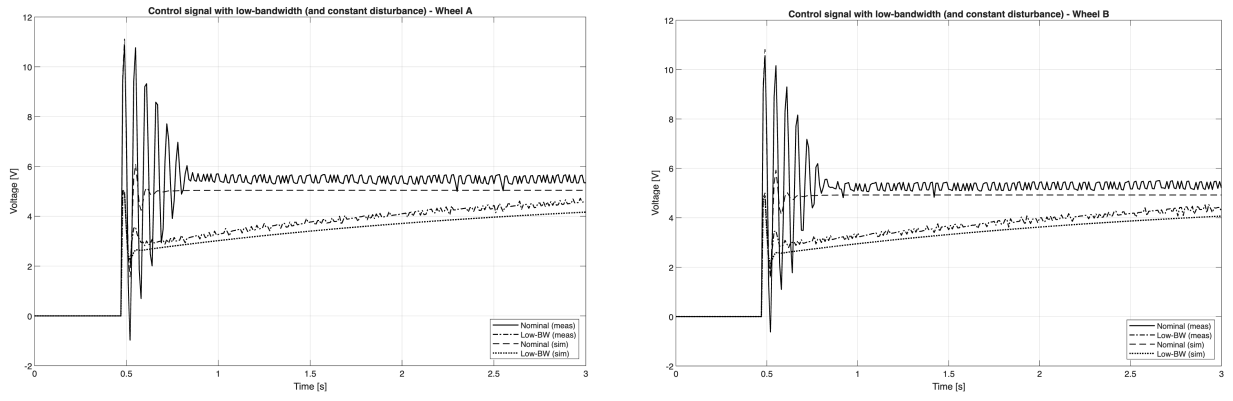
**Control signal with low-bandwidth (and constant disturbance):** Figure 12 shows the control signal comparison for both motor A (left) and motor B (right). The measured and simulated control signal of the step reference are shown in one plot, both for the nominal and low-bandwidth case. The measured control signal of the low-bandwidth controller has clearly smaller peaks and a smoother shape. Although both controllers must compensate the same constant disturbance torque, the low-bandwidth controller converges to a slightly lower steady-state voltage in the measurements, likely due to reduced sensitivity to noise and unmodeled dynamics. The nominal controller generates sharper transients and larger initial control peaks, which push the actuator closer to saturation and amplify noise. The simulated control signals show the same qualitative difference between both designs.

**Contribution of the different (PI) controller parts:** For the nominal design, the proportional term (P) drives rapid acceleration and overshoot, while the integrator (I) eliminates any residual steady-state error under disturbance. In the low-bandwidth design, reduced gain  $K$  and lower  $\omega_c$  cause the proportional action to react more slowly, with the integral term building more gradually. This results in smoother, better-damped responses and lower peak control effort, though convergence to the reference is slower.



(a) Wheel A - Tracking error with low-bandwidth (and constant disturbance)      (b) Wheel B - Tracking error with low-bandwidth (and constant disturbance)

Figure 11: Tracking error comparison for wheel A (left) and wheel B (right): nominal controller vs. low-bandwidth controller, both under constant force disturbance.



(a) Wheel A - Control signal with low bandwidth (and constant disturbance)      (b) Wheel B - Control signal with low-bandwidth (and constant disturbance)

Figure 12: Control voltage comparison for wheel A (left) and wheel B (right): nominal controller vs. low-bandwidth controller, both on the incline.

## References

- [1] Jan Swevers and Goedele Pipeleers. *C8. Control Design Using Frequency Response Methods*. KU Leuven, 2024.

## A Additional figures

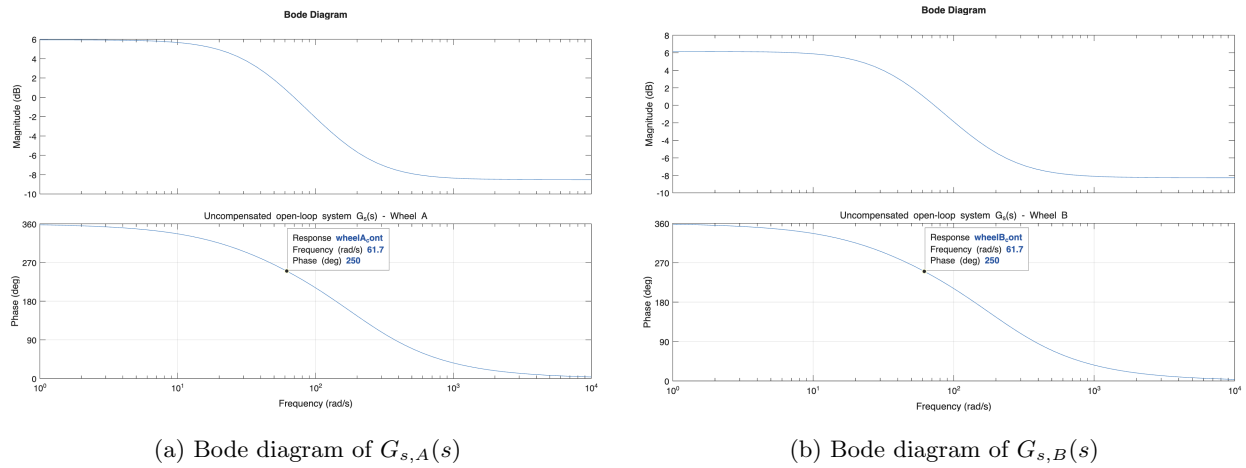
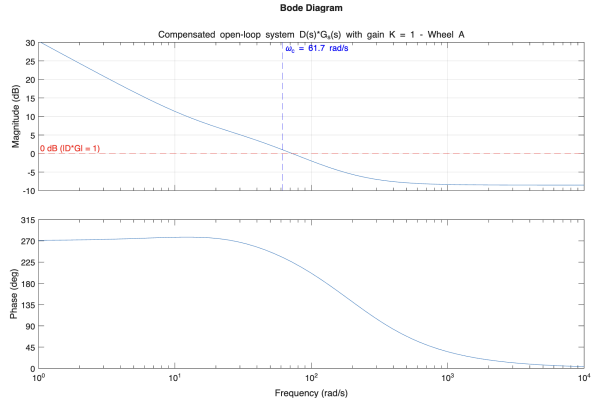
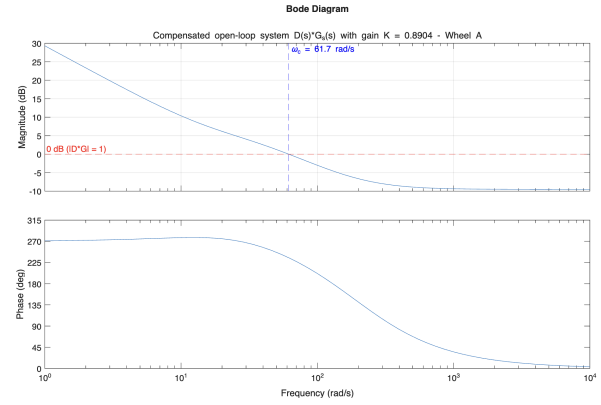


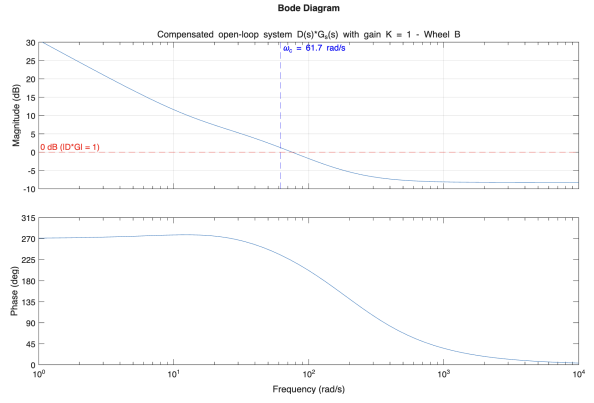
Figure 13: Bode diagram of the uncompensated open-loop system  $G_s(s)$  for wheel A (left) and wheel B (right).



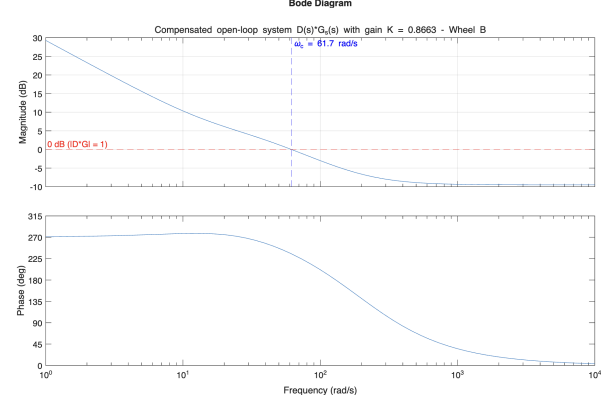
(a) Wheel A - PI compensator has gain  $K_A = 1$



(b) Wheel A - PI compensator has gain  $K_A = 0.8904$



(c) Wheel B - PI compensator has gain  $K_B = 1$



(d) Wheel B - PI compensator has gain  $K_B = 0.8663$

Figure 14: Bode diagram of the compensated open-loop system  $D(j\omega)G_s(j\omega)$  for wheel A (top row) and wheel B (bottom row).